

QP-based refined manipulability-maximizing scheme for coordinated motion planning and control of physically constrained wheeled mobile redundant manipulators

Yunong Zhang · Xiaogang Yan · Dechao Chen · Dongsheng Guo · Weibing Li

Received: 5 February 2015 / Accepted: 12 February 2016 / Published online: 29 February 2016
© Springer Science+Business Media Dordrecht 2016

Abstract By following the pseudoinverse-type formulation, a corresponding quadratic program (QP)-based rough manipulability-maximizing (RoMM) scheme is obtained. In consideration of the drawbacks of the RoMM scheme, a novel QP-based refined manipulability-maximizing (ReMM) scheme is proposed and investigated in this paper for coordinated motion planning and control of a physically constrained wheeled mobile redundant manipulator (WMRM). Such a scheme treats the mobile platform and the redundant manipulator as a combined robotic system, showing an interesting trend of combining motion planning and reactive control methodologically and systematically. In addition, physical limits of mobile manipulators are incorporated into the scheme formulation, which enables the proposed ReMM scheme to keep all the resolved variables within their physical limits. Besides, the proposed ReMM scheme is finally reformulated as a unified QP. For testing the ReMM scheme, the WMRM composed of a two-wheel-drive mobile

platform and a six-degrees-of-freedom manipulator is presented and investigated, together with its kinematics analysis. Comparative simulations performed on such a WMRM substantiate the efficacy, accuracy and superiority of the proposed ReMM scheme, as compared to the RoMM scheme.

Keywords Manipulability maximizing · Coordinated motion planning and control · Wheeled mobile redundant manipulators · Quadratic program

1 Introduction

Recently, robotic researchers have focused on solving a variety of tasks requiring sophisticated motion in complex environments (e.g., working in hazardous or rough-and-tumble environments and exploring unpredictable regions) [1–11]. For a robot manipulator, it is said to be redundant when more degrees-of-freedom (DOF) are available than the minimum number of DOF required to perform a given end-effector primary task [9, 12, 13]. As compared to nonredundant manipulators, redundant manipulators have wider operational space and extra DOF to meet a number of functional constraints. Among such redundant manipulators, fixed-base redundant manipulators are the most frequently encountered ones, which have long been investigated [9, 12–16]. For example, with joint physical limits considered, the repetitive motion planning and control on redundant robot manipulators with push-rod-type

Y. Zhang (✉) · X. Yan · D. Chen · D. Guo · W. Li
School of Information Science and Technology, Sun Yat-sen University (SYSU), Guangzhou 510006, China
e-mail: zhynong@mail.sysu.edu.cn; ynzhang@ieee.org

Y. Zhang · X. Yan · D. Chen · D. Guo · W. Li
SYSU-CMU Shunde International Joint Research Institute,
Shunde 528300, China

Y. Zhang · X. Yan · D. Chen · D. Guo · W. Li
Key Laboratory of Autonomous Systems and Networked Control, Ministry of Education,
Guangzhou 510640, China

joints was studied in [12]. For eliminating the problem of uncompensated dynamics and model uncertainties introduced by the velocity estimator or observer, a robust controller with only joint position feedback was proposed in [14]. Farmanbordar and Hoseini presented a neural network-based adaptive output-feedback control method for flexible link manipulators [15]. Based on the torque-velocity relationship, a manipulability-based approach was presented in [16], where the force effect was taken into consideration. Tanaka et al. [17] proposed a scheme for human force manipulability (HFM) based on the use of isometric joint torque properties to simulate the spatial characteristics of human operation forces at an end-point of a limb with feasible magnitudes for a specified limb posture.

Due to the in-depth research in robotics, mobile robots (including mobile manipulators) have attracted increasing attention [18–28], owing to their combination of mobility and dexterity. For example, the semiglobal stabilization problem for nonholonomic wheeled mobile robots based on dynamic feedback with inputs saturation was considered in [22], where a continuous, bounded and time-varying controller was proposed. In [24] and [25], repeatable inverse kinematics algorithms for mobile manipulators were presented. The modeling of nonholonomic mobile manipulators was investigated in [27], where the standard definition of manipulability was generalized to the case of mobile manipulators. In general, a mobile robot manipulator can be built from a robot manipulator mounted on a mobile platform [27]. The mobile robot manipulator can combine the advantages of the robot manipulator and the mobile platform and reduce their drawbacks [27]. If the manipulator equipped on the mobile platform is redundant, such a mobile manipulator would possess both the superiorities of the mobile platform and those of the redundant manipulator. Thus, the mobile redundant manipulator, which can achieve coordinated movements of the mobile platform and the redundant manipulator, is superior to the fixed-base one. In this paper, a wheeled mobile redundant manipulator (WMRM) composed of a two-wheel-drive mobile platform and a six-DOF manipulator is presented and investigated, together with its kinematics analysis.

Generally speaking, for mobile redundant manipulators, one fundamental issue in controlling and coordinating locomotion and manipulation is to design suitable redundancy-resolution approaches (such that the

coordinated motion planning and control of mobile redundant manipulators can be achieved). In the past few decades, many efforts have been contributed to the motion planning of mobile redundant manipulators, and subsequently lots of schemes have been proposed and investigated for mobile redundant manipulators [24–31]. In other words, the studies on motion planning of mobile (redundant) manipulators have achieved quite great development. Note that the basic research methodology is to find an optimal solution to the robotic kinematics by designing various performance criteria [31].

Among such performance criteria, a representative performance criterion is the maximizing of the manipulators' manipulability [16,27,29,30], which is proposed and investigated for solving the so-called singularity problem arising in the motion planning and control of manipulators. It is worth pointing out that when the manipulator is at a kinematic singularity configuration, the Jacobian matrix of the manipulator becomes ill-conditioned and rank-deficient. This would result in the failure of the end-effector movement in a certain direction. As a matter of fact, getting close to a singularity point of the kinematic mapping is also undesirable (or say, unacceptable). This is because that, in such a state, when the end-effector moves in certain directions, joint velocities and accelerations can be arbitrarily large [32,33], which would cause damage to the physical manipulator. Thus, maximizing the manipulability of manipulators has explicit significance when it is related to singularity avoidance. Besides, the manipulability-maximizing performance criteria reflect the manipulator's ability in converting the motion of the joint. Due to its important role, many studies have been reported on the redundancy resolution of robot manipulators through the manipulability maximizing [27,29,30,32–38]. The initial study was conducted by Yoshikawa [32], who proposed the quantitative measure of the manipulability at the joint state θ for fixed-base redundant manipulators. Specifically, the manipulability measure is expressed in the following explicit form:

$$M(\theta) = \sqrt{\det(J(\theta)J^T(\theta))}, \quad (1)$$

where $\det(\cdot)$ denotes the determinant of a matrix, $J(\theta)$ is the Jacobian matrix, and superscript T denotes the transpose of a matrix or vector. Note that the

pseudoinverse-type algorithm proposed in [32] aims at the singularity avoidance of fixed-base redundant manipulators by maximizing the manipulability measure $M(\theta)$. Bayle et al. [27] extended the theory of manipulability to the case of wheeled mobile manipulators and pointed out some possible applications of such instantaneous kinematic analysis from a control point of view. Huang et al. [34] investigated the motion planning of mobile manipulators concerning the platform stability and the manipulator manipulability simultaneously. In literature [34], the end-effector path and platform motion were firstly planned and given, and then the manipulator configuration was computed by means of the manipulability maximizing. Note that most of the aforementioned methods and techniques are based on pseudoinverse-type formulations and do not consider physical limits of mobile manipulators.

In view of the fact that physical limits always exist in a practical mobile manipulator, it is meaningful to analyze and investigate the physically constrained mobile manipulators (with manipulability maximizing). Take a wheeled mobile manipulator as an example. Physical limits generally include the joint-angle and joint-velocity limits of the manipulator as well as the rotational velocity limits of the wheels. Note that it is difficult to incorporate physical limits into pseudoinverse-type formulations. To avoid all the physical limits, a sweaty and boring derivation process of the complex optimization criterion is inevitable, not to mention determining the magnitude of some related parameters based on trial-and-error approaches. Thus, it is necessary to develop a scheme that can handle the physical limits readily for physically constrained mobile manipulators.

Inspired by the successful work [39–41], by following the pseudoinverse-type formulation, we present a quadratic program (QP)-based rough manipulability-maximizing (RoMM) scheme. In view of the drawbacks of the RoMM scheme, a novel QP-based refined manipulability-maximizing (ReMM) scheme is thus proposed and investigated in this paper for the coordinated motion planning and control of physically constrained WMRM. Such a scheme, which treats the mobile platform and the redundant manipulator as a combined robotic system, is reformulated into a unified QP. Note that the QP can be converted into a linear variational inequality (LVI), and the resultant LVI is equivalent to a piecewise-linear equation (PLE) which

can be solved by many algorithms and techniques efficiently, such as numerical methods [12,42] and recurrent neural networks [13,43]. In this paper, the LVI-based primal-dual neural network [13,43] is exploited for online solution of the QP problem, as well as the proposed ReMM scheme. Comparative simulation results based on the presented physically constrained WMRM (with its kinematics analysis discussed in the ensuing section) further substantiate the efficacy, accuracy and superiority of the proposed ReMM scheme. To the best of the authors' knowledge, the proposed ReMM scheme for physically constrained mobile manipulators has never been investigated in the existing literature.

The remainder of this paper is organized as follows. In Sect. 2, the WMRM composed of a two-wheel-drive mobile platform and a six-DOF manipulator is presented and discussed, together with its kinematics analysis. Section 3 proposes and investigates the ReMM scheme for the coordinated motion planning and control of WMRM, which is reformulated as a unified QP in Sect. 4. In Sect. 5, comparative simulation results are shown for the WMRM under the presented RoMM scheme and under the proposed ReMM scheme. Observations and comparisons are also illustrated. Section 6 concludes this paper with final remarks. Before ending this introductory section, it is worth mentioning the main contributions of this paper as follows.

- (1) The kinematics analysis of the wheeled mobile six-DOF manipulator is presented, from which a combined forward-kinematics equation is derived. Note that the rotational velocities of the wheels and joint velocities of the manipulator can be obtained simultaneously by solving such an equation.
- (2) A novel ReMM scheme is proposed and investigated for the coordinated motion planning and control of physically constrained WMRM. In addition, such a scheme is reformulated as a QP problem, which is solved via the LVI-based primal-dual neural network [13,43]. To the best of the authors' knowledge, the proposed ReMM scheme for mobile manipulators has never been investigated in existing literature.
- (3) Comparative simulations performed on such a WMRM demonstrate the efficacy, accuracy and superiority of the proposed ReMM scheme, as compared to the RoMM scheme.

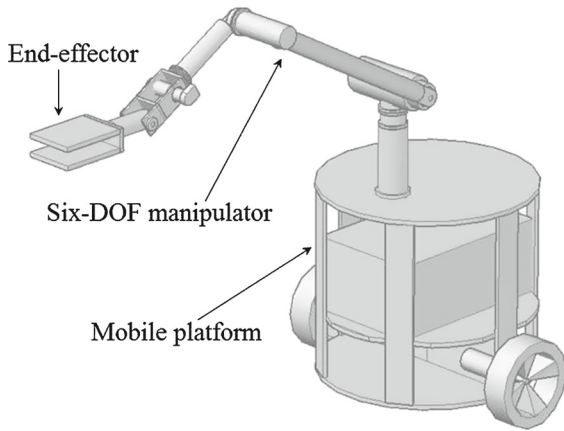


Fig. 1 CAD model of the wheeled mobile redundant manipulator

2 Wheeled mobile redundant manipulator

In this section, the kinematics analysis of the WMRM is presented for further investigation. The computer-aided design (CAD) model of such a mobile manipulator is shown in Fig. 1. Evidently, as seen from Fig. 1, the WMRM is composed of a two-wheel-drive mobile platform and a six-DOF manipulator. Thus, the kinematics equation of the wheeled mobile redundant manipulator is obtained based on the kinematics of the wheeled mobile platform and that of the six-DOF manipulator discussed in the following subsections.

2.1 Wheeled mobile platform kinematics

In this subsection, the kinematics of the wheeled mobile platform is discussed for the mobile manipulator shown in Fig. 1. Note that such a mobile platform has two independently driving wheels (and two passive omnidirectional supporting wheels), with its simplified model illustrated in Fig. 2. To lay a basis for further discussion, the radius of each driving wheel of the mobile platform is denoted as γ , and $\dot{\varphi}_L$ and $\dot{\varphi}_R$ denote the left and right driving wheels' angular speeds, respectively. Thus, the driving wheels' angular speed vector is $\dot{\phi} = [\dot{\varphi}_L \ \dot{\varphi}_R]^T$, and the corresponding angle (angular position) vector is $\phi = [\varphi_L \ \varphi_R]^T$. Besides, some descriptions about the two-wheel-drive mobile platform shown in Fig. 2 are given in Table 1.

It is worth pointing out here that, in this paper, we only consider the motion of the mobile platform in the

horizontal plane [9, 27, 28]. As shown in Fig. 2 (where $\dot{z}_G = 0$), in the $X^wO^wY^w$ plane of $\{w\}$, the motion of the mobile platform (as a rigid body) can be viewed as a rotation about the instantaneous center Q . Under the assumption that no-slipping and no-sideways sliding occur to the platform [9, 27, 28], the velocities of points A and B are both strictly perpendicular to the driving wheel axle. Thus, the instantaneous center Q must locate at the driving wheel axle or its extended line, as shown in Fig. 2. Then, the angular velocity, at which the mobile platform is rotating about Q , is exactly $\dot{\phi}$.

Based on the above analysis, inspired by [9, 27, 28], we can have

$$\dot{\phi} = \frac{\gamma \dot{\varphi}_L}{\gamma} = \frac{\gamma \dot{\varphi}_R}{\gamma + 2b} = \frac{\dot{x}_G c_\phi + \dot{y}_G s_\phi}{\gamma + b}, \tag{2}$$

and

$$\dot{y}_G c_\phi = d\dot{\phi} + \dot{x}_G s_\phi, \tag{3}$$

where $c_\phi = \cos \phi$, $s_\phi = \sin \phi$, and γ is the length of line segment AQ . By following (2) and (3), the kinematics equation of the mobile platform can be reformulated as

$$\dot{P}_G = \begin{bmatrix} \dot{x}_G \\ \dot{y}_G \\ \dot{z}_G \end{bmatrix} = \begin{bmatrix} \frac{\gamma}{2} c_\phi + \frac{\gamma d}{2b} s_\phi & \frac{\gamma}{2} c_\phi - \frac{\gamma d}{2b} s_\phi \\ \frac{\gamma}{2} s_\phi - \frac{\gamma d}{2b} c_\phi & \frac{\gamma}{2} s_\phi + \frac{\gamma d}{2b} c_\phi \\ 0 & 0 \end{bmatrix} \begin{bmatrix} \dot{\varphi}_L \\ \dot{\varphi}_R \end{bmatrix},$$

$$\text{and } \dot{\phi} = \begin{bmatrix} -\frac{\gamma}{2b} & \frac{\gamma}{2b} \end{bmatrix} \begin{bmatrix} \dot{\varphi}_L \\ \dot{\varphi}_R \end{bmatrix}.$$

2.2 Six-DOF manipulator kinematics

The six-DOF manipulator mounted on the mobile platform is shown in Fig. 3. In this subsection, the kinematics of the manipulator is also presented.

In general, the functional relation between the end-effector position/orientation vector $r_0(t) \in R^m$ in Cartesian space with respect to the base coordinate frame and the joint-angle vector $\theta(t) \in R^n$ in joint space can be written readily as $r_0 = f(\theta)$, where $f(\cdot)$ denotes a differentiable nonlinear mapping. According to some researches on the kinematics of (fixed-base) robot manipulators [9, 12], the specific kinematics equation of the six-DOF manipulator shown in Fig. 3 is presented directly as follows:

Fig. 2 Simplified model of the two-wheel-drive mobile platform

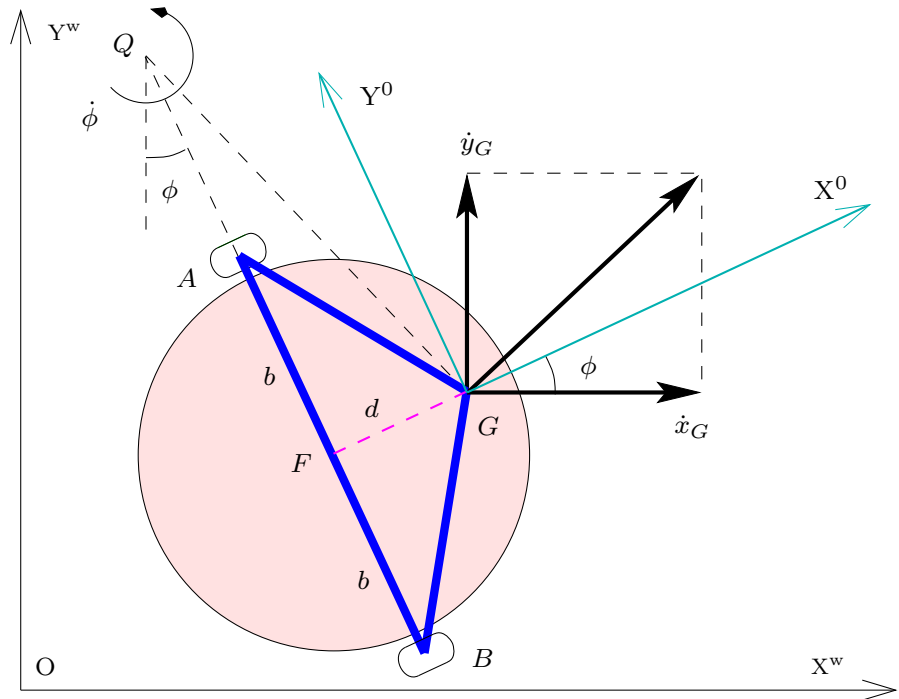


Table 1 Some descriptions for the two-wheel-drive mobile platform shown in Fig. 2

Symbol	Description
A	Center point of the left driving wheel
B	Center point of the right driving wheel
F	Midpoint of line segment AB , and $AF = FB = b$
G	Manipulator's base location, which is at the midperpendicular of AB
$X^0 Y^0 Z^0$	Coordinate frame attached to mobile platform, which is denoted as $\{0\}$
$X^w Y^w Z^w$	World coordinate frame, which is denoted as $\{w\}$
ϕ	Orientation angle of mobile platform with $\dot{\phi}$ being its time derivative
$[\dot{x}_G \ \dot{y}_G \ \dot{z}_G]^T$	Velocity vector of point G in $\{w\}$
d	Length of line segment FG

$$r_0 = f(\theta) = \begin{bmatrix} l_{65}(c_5 s_{32} c_1 - s_5 c_4 c_{32} c_1 + s_5 s_4 s_1) + l_{43} s_{32} c_1 + l_2 s_2 c_1 \\ l_{65}(c_5 s_{32} s_1 - s_5 c_4 c_{32} s_1 - s_5 s_4 c_1) + l_{43} s_{32} s_1 + l_2 s_2 s_1 \\ l_{65}(s_5 c_4 s_{32} + c_5 c_{32}) + l_{43} c_{32} + l_2 c_2 + l_1 + l_0 \end{bmatrix}, \tag{4}$$

where $c_i = \cos(\theta_i)$ and $s_i = \sin(\theta_i)$ with $i = 1, 2, \dots, 6$. Besides, $l_{65} = (l_6 + l_5)$, $l_{43} = (l_4 + l_3)$, $s_{32} = \sin(\theta_3 + \theta_2)$ and $c_{32} = \cos(\theta_3 + \theta_2)$. In addition, $l_0 = 0.698$ m denotes the distance between Joint 1 and the ground. The specific values of parameters (for the six-DOF manipulator shown in Fig. 3) are $l_1 = 0.065$

m, $l_2 = 0.555$ m, $l_3 = 0.19$ m, $l_4 = 0.13$ m, $l_5 = 0.082$ m, and $l_6 = 0.133$ m.

2.3 WMRM kinematics

In this subsection, the kinematics equation of the WMRM shown in Fig. 1 is developed based on those of the mobile platform and the six-DOF manipulator, i.e., the integrated kinematics for the WMRM.

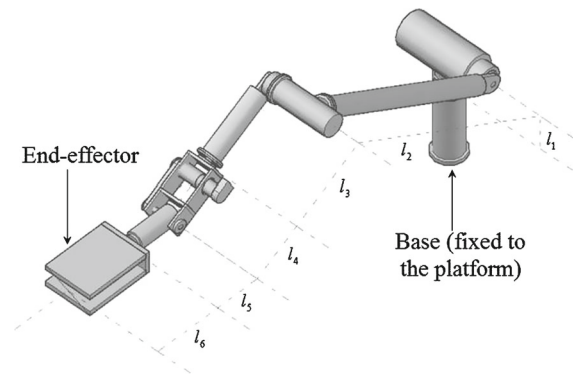


Fig. 3 CAD model of the six-DOF manipulator

The homogeneous coordinate transformation matrix from the mobile platform coordinate frame $\{0\}$ to the world coordinate frame $\{w\}$ is given as follows:

$${}^w_0T = \begin{bmatrix} c_\phi & -s_\phi & 0 & x_G \\ s_\phi & c_\phi & 0 & y_G \\ 0 & 0 & 1 & 0 \\ 0 & 0 & 0 & 1 \end{bmatrix},$$

where x_G and y_G represent, respectively, the magnitude components of point G in the X^w - and Y^w -axis directions shown in Fig. 2. In other words, $[x_G \ y_G]^T$ is the position vector of point G in the X^wOY^w plane of $\{w\}$ (as shown in Fig. 2). Based on (4), the homogeneous coordinate of the end-effector with respect to $\{w\}$ can be obtained as

$$\begin{bmatrix} r_w \\ 1 \end{bmatrix} = {}^w_0T \begin{bmatrix} r_0 \\ 1 \end{bmatrix} = [r_{wX} \ r_{wY} \ r_{wZ} \ 1]^T, \tag{5}$$

where $r_{wX} = x_G + l_6(s_5s_3c_1\phi - s_5c_4c_3c_1\phi + s_5s_4s_1\phi) + l_4s_3c_1\phi + l_2s_2c_1\phi$, $r_{wY} = y_G + l_6(c_5s_3s_1\phi - s_5c_4c_3s_1\phi - s_5s_4c_1\phi) + l_4s_3s_1\phi + l_2s_2s_1\phi$, and $r_{wZ} = l_6(s_5c_4s_3c_2 + c_5c_3c_2) + l_4c_3c_2 + l_2c_2 + l_1 + l_0$, with $s_1\phi = \sin(\theta_1 + \phi)$ and $c_1\phi = \cos(\theta_1 + \phi)$. By defining the augmented variable vector $p = [x_G \ y_G \ \phi \ \theta^T]^T \in R^{3+n}$ (viewed as the state vector of the wheeled mobile manipulator), it follows from the aforementioned analysis, the kinematics equation of the wheeled mobile manipulator at the position level is formulated as

$$r_w = g(p),$$

where $g(\cdot)$ is a differentiable nonlinear mapping, which is similar to $f(\cdot)$.

Furthermore, let $q(t) = [\varphi^T(t) \ \theta^T(t)]^T \in R^{2+n}$ denote the combined angle vector, and $\dot{q}(t) = [\dot{\varphi}^T(t) \ \dot{\theta}^T(t)]^T$ denote the time derivative of $q(t)$ (i.e., the combined velocity vector). Then, the mobile manipulator’s motion planning/coordinated control is to generate $q(t)$ or $\dot{q}(t)$ for the driving wheels and joints, so that the end-effector of the mobile manipulator can move along the desired Cartesian path $r_{dw}(t) \in R^m$ in $\{w\}$. By differentiating (5) with respect to time t , the kinematics equation of wheeled mobile manipulator at the velocity level is thus obtained as

$$\dot{r}_w = J(\vartheta)\dot{q}, \tag{6}$$

where \dot{r}_w denotes the time derivative of r_w , and the matrix $J(\vartheta) \in R^{m \times (2+n)}$ (which, hereafter, is rewritten as J for simplicity) with the vector $\vartheta = [\phi \ \theta^T]^T \in R^{1+n}$. For the detailed expression about J , please see the “Appendix”. Note that such an integrated kinematics depicted in (5) or (6) might give us new insights to the coordinated control of the mobile manipulators (since there are lots of work on redundancy resolution of fixed-base manipulators [9, 12, 13, 39–41]), e.g., manipulability maximizing presented in the ensuing section.

3 Scheme formulation and efficacy analysis

In this section, on the basis of (6), by following the pseudoinverse-type formulation, a novel manipulability-maximizing scheme (i.e., the ReMM scheme) for the WMRM is proposed and investigated. Besides, the efficacy analysis of such an ReMM scheme is presented as well.

3.1 Scheme formulation

To achieve the purpose of motion planning of the WMRM, based on (6), a general pseudoinverse-type scheme at the velocity level is formulated as

$$\dot{q} = P\dot{r}_{dw} + (I - PJ)\xi, \tag{7}$$

where $P \in R^{(2+n) \times m}$ denotes the pseudoinverse of J , $\dot{r}_{dw} \in R^m$ denotes the time derivative of the desired Cartesian path r_{dw} , and $I \in R^{(2+n) \times (2+n)}$ denotes the identity matrix. In addition, $\xi \in R^{2+n}$ is an arbitrary vector usually selected by using some optimization criteria (e.g., the manipulability maximizing). For better

mathematical tractability, differing from the manipulability measure depicted in (1), $w = \det(JJ^T)$ is used as a new manipulability measure in this paper. To maximize the manipulability measure, ξ in (7) can be chosen as the positive gradient of w , i.e., $\xi = v\partial w/\partial q$ with $v > 0$ being a constant scalar. Thus, we can have the following pseudoinverse-type scheme for maximizing the manipulability measure w :

$$\dot{q} = P\dot{r}_{dw} + v(I - PJ)\frac{\partial w}{\partial q}, \tag{8}$$

where the i th [with $i = 1, 2, \dots, (2 + n)$] element of $\partial w/\partial q$, i.e., ξ_i , is given mathematically as

$$\begin{aligned} \xi_i &= \frac{\partial \det(JJ^T)}{\partial q_i} = \det(JJ^T) \text{ trace} \\ &\left((JJ^T)^{-1} \frac{\partial (JJ^T)}{\partial q_i} \right) = \det(JJ^T) \text{ trace} \\ &\left((JJ^T)^{-1} \left(\frac{\partial J}{\partial q_i} J^T + J \left(\frac{\partial J}{\partial q_i} \right)^T \right) \right), \end{aligned}$$

with $\text{trace}(\cdot)$ denoting the trace of a matrix argument.

For (8), on the one hand, the first part of the right side represents the particular solution (i.e., the minimum Euclidean-norm solution) to the velocity-level kinematics equation (6). On the other hand, the rest part represents the homogeneous solution, which can achieve the manipulability maximizing. Therefore, the pseudoinverse-type scheme (8) can be viewed as the combination of the minimum velocity norm (MVN) solution and the manipulability-maximizing solution. By understanding this point and considering the physical limits of the mobile manipulator, the novel ReMM scheme for the coordinated motion planning and control of WMRM is proposed as

$$\text{minimize } \frac{1}{2} \|\dot{\theta}\|_2^2 - \xi^T \dot{q} \tag{9}$$

$$\text{subject to } J\dot{q} = \dot{r}_{dw} + \kappa(r_{dw} - g(p)), \tag{10}$$

$$q^- \leq q \leq q^+, \tag{11}$$

$$\dot{q}^- \leq \dot{q} \leq \dot{q}^+, \tag{12}$$

$$\text{with } \xi = v\partial w/\partial q, \tag{13}$$

where $\|\cdot\|_2$ denotes the two norm of a vector, $\dot{\theta}$ denotes the joint-velocity vector of the six-DOF manipulator. In consideration of the modeling errors and computational round-off errors, the position feedback is elegantly added to (10), i.e., $\dot{r}_{dw} + \kappa(r_{dw} - g(p))$, where

Table 2 Physical limits of the wheeled mobile manipulator

i	q_i^- (rad)	q_i^+ (rad)	\dot{q}_i^- (rad/s)	\dot{q}_i^+ (rad/s)
1	$-\infty$	$+\infty$	-25	25
2	$-\infty$	$+\infty$	-25	25
3	$-\pi/12$	$\pi/4$	-3	3
4	$\pi/12$	$5\pi/12$	-3	3
5	$-\pi/24$	$\pi/3$	-3	3
6	$-\pi/12$	$\pi/4$	-3	3
7	$-\pi/6$	$\pi/4$	-3	3
8	$-\pi/4$	$\pi/12$	-3	3

$\kappa > 0 \in R$ is the feedback gain. In addition, q^- and q^+ (\dot{q}^- and \dot{q}^+) denote the lower and upper limits of the combined angle vector q (the combined velocity vector \dot{q}), respectively. For convenience, the physical limits (i.e., q^-, q^+, \dot{q}^- and \dot{q}^+) of the wheeled mobile manipulator used in this paper are listed in Table 2.

3.2 Efficacy analysis

By understanding the nature of the pseudoinverse-type scheme (8), according to the well-known gradient method, if $\dot{q} = v\partial w/\partial q = v\partial \det(JJ^T)/\partial q$, then the redundant DOF of the mobile manipulator can be utilized to achieve high manipulability during the end-effector task execution. In other words, w can be maximized when $\dot{q} = v\partial w/\partial q$. Note that such a dynamic equation is achieved theoretically.

Based on the authors' previous works [2,3,12] on the quadratic programming technique for redundancy resolution, we define $\hat{e} = \dot{q} - \xi$ with $\xi = v\partial w/\partial q$. Therefore, minimizing $\|\hat{e}\|_2^2/2$ appears to be more feasible, rather than forcing $\dot{q} - \xi = 0$ directly in its exact form. It is worth pointing out here that the minimization of $\|\hat{e}\|_2^2/2$ is equivalent to the maximizing of w . Expanding $\|\hat{e}\|_2^2/2$, we have

$$\begin{aligned} \|\hat{e}\|_2^2/2 &= \dot{q}^T \dot{q} / 2 - \xi^T \dot{q} + \xi^T \xi / 2 \\ &= \|\dot{q}\|_2^2 / 2 - \xi^T \dot{q} + \|\xi\|_2^2 / 2. \end{aligned} \tag{14}$$

Since the motion of wheeled mobile manipulator is planned at velocity level, the decision-variable vector is \dot{q} . Subsequently, the function ξ (i.e., $\xi = v\partial w/\partial q$) is viewed as a constant in the performance index (14) (with respect to \dot{q}). In addition, $\|\xi\|_2^2/2$ is positive and viewed as a constant (with respect to \dot{q} as well), which is

thus set aside from the performance index (14). Therefore, to maximize the manipulability of physically constrained WMRM, the following rough manipulability-maximizing scheme (i.e., the RoMM scheme) can be obtained directly:

$$\text{minimize } \frac{1}{2} \|\dot{q}\|_2^2 - \xi^T \dot{q} \quad (15)$$

$$\text{subject to } J\dot{q} = \dot{r}_{dw} + \kappa(r_{dw} - g(p)), \quad (16)$$

$$q^- \leq q \leq q^+, \quad (17)$$

$$\dot{q}^- \leq \dot{q} \leq \dot{q}^+, \quad (18)$$

Note that, for the coordinated motion planning and control of WMRM (e.g., the one shown in Fig. 1), in view of the computational complexity, it may be less necessary to consider the motion of the driving wheels in the minimum norm form (i.e., $\|\dot{\phi}\|_2^2/2$). Thus, we would like to exploit the minimization of $\|\dot{\theta}\|_2^2/2$ instead of the minimization of $\|\dot{q}\|_2^2/2$ for the coordinated motion planning and control of WMRM. Besides, it is also worth pointing out that the comparative simulation results (given in Sect. 5) validate that the minimization of $\|\dot{\theta}\|_2^2/2 - \xi^T \dot{q}$ [i.e., the performance index (9)] outperforms that of $\|\dot{q}\|_2^2/2 - \xi^T \dot{q}$ [i.e., the performance index (15)] in terms of maximizing the manipulability of WMRM.

Therefore, based on the above analysis, by setting $\|\dot{\phi}\|_2^2/2$ and $\|\xi\|_2^2/2$ from (14), the new performance index (9) is obtained. Furthermore, by introducing the position feedback and considering the physical limits, we have the equality constraint (10) and bound constraints (11) and (12). The efficacy analysis of the proposed ReMM scheme for maximizing the manipulability is thus complete.

Remark 1 The refined manipulability-maximizing (ReMM) scheme and the rough manipulability-maximizing (RoMM) scheme are two different schemes with different performance indices [i.e., (9) for the ReMM scheme and (15) for the RoMM scheme]. Note that the ReMM scheme and the RoMM scheme are both reformulated as the QP problems in this paper. Thus, the QP is not the factor that makes the ReMM scheme better than the RoMM scheme. Rigorously speaking, it is the novel performance index (9) that makes the ReMM scheme better than the RoMM scheme in terms of the computational complexity for the scheme and the manipulability maximizing for the WMRM.

4 Scheme unification

According to [12, 13], physical limits (11) and (12) can be combined as $\varsigma^- \leq \dot{q} \leq \varsigma^+$, with the i th elements of ς^- and ς^+ being, respectively, defined as $\varsigma_i^- = \max\{\mu(q_i^- - q_i), \dot{q}_i^-\}$ and $\varsigma_i^+ = \min\{\mu(q_i^+ - q_i), \dot{q}_i^+\}$ (in which $i = 1, 2, 3, \dots, 2+n$). In addition, the design parameter $\mu > 0 \in R$ is used to scale the feasible region of \dot{q} .

Then, by defining the decision-variable vector $x = \dot{q}$ and setting $\|\dot{\phi}\|_2^2/2$ as well as $\|\xi\|_2^2/2$ from (14), the proposed ReMM scheme (9)–(12) is reformulated and unified as the following QP:

$$\text{minimize } \frac{1}{2} x^T \hat{Q} x - \hat{p}^T x \quad (19)$$

$$\text{subject to } Jx = \hat{d}, \quad (20)$$

$$\varsigma^- \leq x \leq \varsigma^+, \quad (21)$$

where coefficients are defined as follows:

$$\hat{Q} = \begin{bmatrix} 0 & 0 \\ 0 & I \end{bmatrix} \in R^{(2+n) \times (2+n)}, \quad \hat{p} = \xi \in R^{2+n},$$

$$\hat{d} = \dot{r}_{dw} + \kappa(r_{dw} - g(p)),$$

with the identity matrix $I \in R^{n \times n}$. Note that the QP reformulation and unification can not only make a better understanding of the previous and current work on redundancy resolution of robot manipulators, but also give us many new insights to the motion planning of (mobile) redundant manipulators in the future robotic research. These are the reasons why we tend to develop a rich repertoire of QP-based schemes [12, 13, 39–41] for redundant robot manipulators. Besides, for online solution of the QP problem, lots of recurrent neural networks have been proposed, developed and investigated [13, 43]. Thus, in this paper, the primal-dual neural network based on linear variational inequality (LVI) [13, 43] is exploited for solving QP (19)–(21). Hereafter, (19)–(21) is termed the ReMM scheme for presentation convenience.

Remark 2 Unlike the conventional pseudoinverse-type form (7), the proposed ReMM scheme (19)–(21) is depicted readily in a more concise optimization form, which can realize the coordinated movements of the mobile platform and the manipulator. In addition, differing from the pseudoinverse-type scheme (8), the proposed scheme can plan the manipulability-maximizing motion of the WMRM with physical limits considered, which is more reasonable in practical applications. In summary, the proposed ReMM scheme is

superior to the scheme (8). More importantly, such an ReMM scheme shows an interesting trend of mixing motion planning and reactive control methodologically and systematically, which is becoming more and more important in the field of automatic control and robotics.

Remark 3 It is worth pointing out here that the significance of the QP for the reformulation of the proposed ReMM scheme lies in the following facts. Firstly, the proposed QP-based ReMM scheme (19)–(21) can avoid solving for Jacobian pseudoinverse [44], and thus it costs considerably less time to solve the same problem than the pseudoinverse-type scheme (8). In other words, the QP-based ReMM scheme (19)–(21) has the relatively low computational complexity. Secondly, the QP-based scheme can handle one-sided inequality constraints and bound constraints (i.e., two-sided inequality constraints), which means that the QP-based scheme can handle other subtasks when the robot manipulator executes the primary task [3]. Finally, for online solution of the QP problem, lots of recurrent neural networks have been proposed, developed and investigated in the recent years [13,43,45], due to their parallel-processing and adaptive-tuning nature [46].

5 Effective verifications

In this section, simulations based on the presented WMRM are performed to verify the efficacy, accuracy and superiority of the proposed ReMM scheme (19)–(21). For comparison, the RoMM scheme (15)–(18) is also simulated. Note that, in the simulations, $x_G(0) = y_G(0) = 0$ m, $\phi(0) = \pi/3$ and $\theta(0) = [\pi/12, \pi/4, \pi/6, \pi/12, \pi/12, -\pi/12]^T$ rad are used for the wheeled mobile manipulator. In addition, the feedback gain $\kappa = 1$ and the task duration $T = 20$ s.

5.1 Tricuspid-curve path-tracking task

For validating the superior performance of the proposed ReMM scheme (19)–(21), comparative simulations are performed on the presented WMRM in this subsection. That is, the RoMM scheme and the ReMM scheme are comparatively applied to the WMRM in order for the manipulator’s end-effector to follow a same tricuspid-curve path. Specifically, the desired velocities of the end-effector for completing such a tracking task are described as

$$\begin{cases} \dot{r}_{dwX} = -\alpha \frac{2\pi^2}{T} \sin\left(\frac{\pi t}{T}\right) (\sin(\beta) + \sin(2\beta)), \\ \dot{r}_{dwY} = \alpha \frac{2\pi^2}{T} \sin\left(\frac{\pi t}{T}\right) (\cos(\beta) - \cos(2\beta)) \cos(\pi/20), \\ \dot{r}_{dwZ} = \alpha \frac{2\pi^2}{T} \sin\left(\frac{\pi t}{T}\right) (\cos(\beta) - \cos(2\beta)) \sin(\pi/20), \end{cases}$$

where $\alpha = 0.25$ and $\beta = 2\pi \sin^2(\pi t/(2T))$.

5.1.1 Simulation results under RoMM scheme

Specifically, Fig. 4 illustrates the simulation results synthesized by the RoMM scheme (15)–(18), when the manipulator’s end-effector tracks the tricuspid-curve path. Evidently, Fig. 4a shows that the path-tracking task is completed well owing to the coordinated movements of the mobile platform and the manipulator. However, as seen from Fig. 4b, the generated maximal absolute value of the position error $\epsilon = r_{dw} - g(p)$ is around 6×10^{-3} m, which is too large to meet the requirement of practical applications. As shown in Fig. 4c, during $t \in [4.8, 9]$ and $[11, 12]$ s, the manipulability measure $w = \det(JJ^T)$ of the whole mobile manipulator system is quite small (specifically, around 0.004), and the manipulability measure $w_{arm} = \det(J_{arm}J_{arm}^T)$ [with $J_{arm} = \partial f(\theta)/\partial \theta$] of the six-DOF manipulator is about zero. This means that there exists the singularity problem (which corresponds to the situation of $w_{arm} = 0$) in the motion of the mobile manipulator. Such a singularity problem is undesirable and unacceptable in practice, which would result in the failure of the path-tracking task, and, sometimes, the damage of the mobile manipulator. In addition, profiles of joint angles are presented in Fig. 4d–f. As illustrated in Fig. 4d–f, except that the joint angle θ_6 is kept within its physical limits, all the other joint angles reach but not exceed their limits during some time periods of the task execution process. These results show that the bound constraints (17) and (18) are effective and activated during the motion. In summary, Fig. 4 indicates that the RoMM scheme (15)–(18) is undesirable and unacceptable for the WMRM in view of large end-effector position error and unexpected singularity problem. Therefore, an effective motion planner (e.g., the proposed ReMM scheme) appears to be needed for avoiding the aforementioned undesirable phenomena.

5.1.2 Simulation results under ReMM scheme

The simulation results synthesized by the proposed ReMM scheme (19)–(21) are shown in Figs. 5 and 6. Specifically, Fig. 5a illustrates the top view of motion

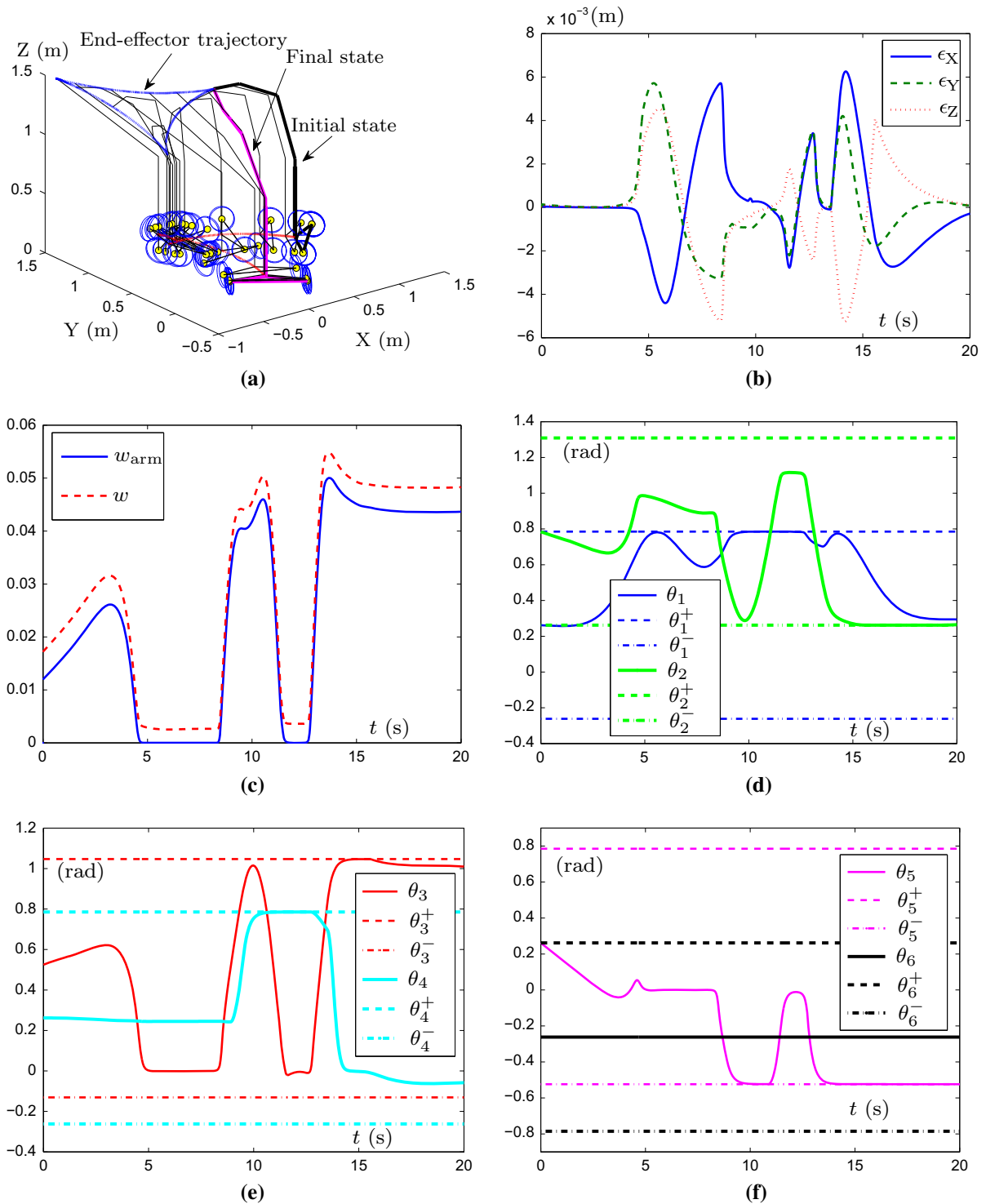


Fig. 4 The WMRM end-effector moves along a tricuspid-curve path, as synthesized by the RoMM scheme (15)–(18). **a** Motion trajectories. **b** Position error ϵ profiles. **c** Manipulability mea-

asures. **d** Joint angle θ_1 and θ_2 profiles. **e** Joint angle θ_3 and θ_4 profiles. **f** Joint angle θ_5 and θ_6 profiles

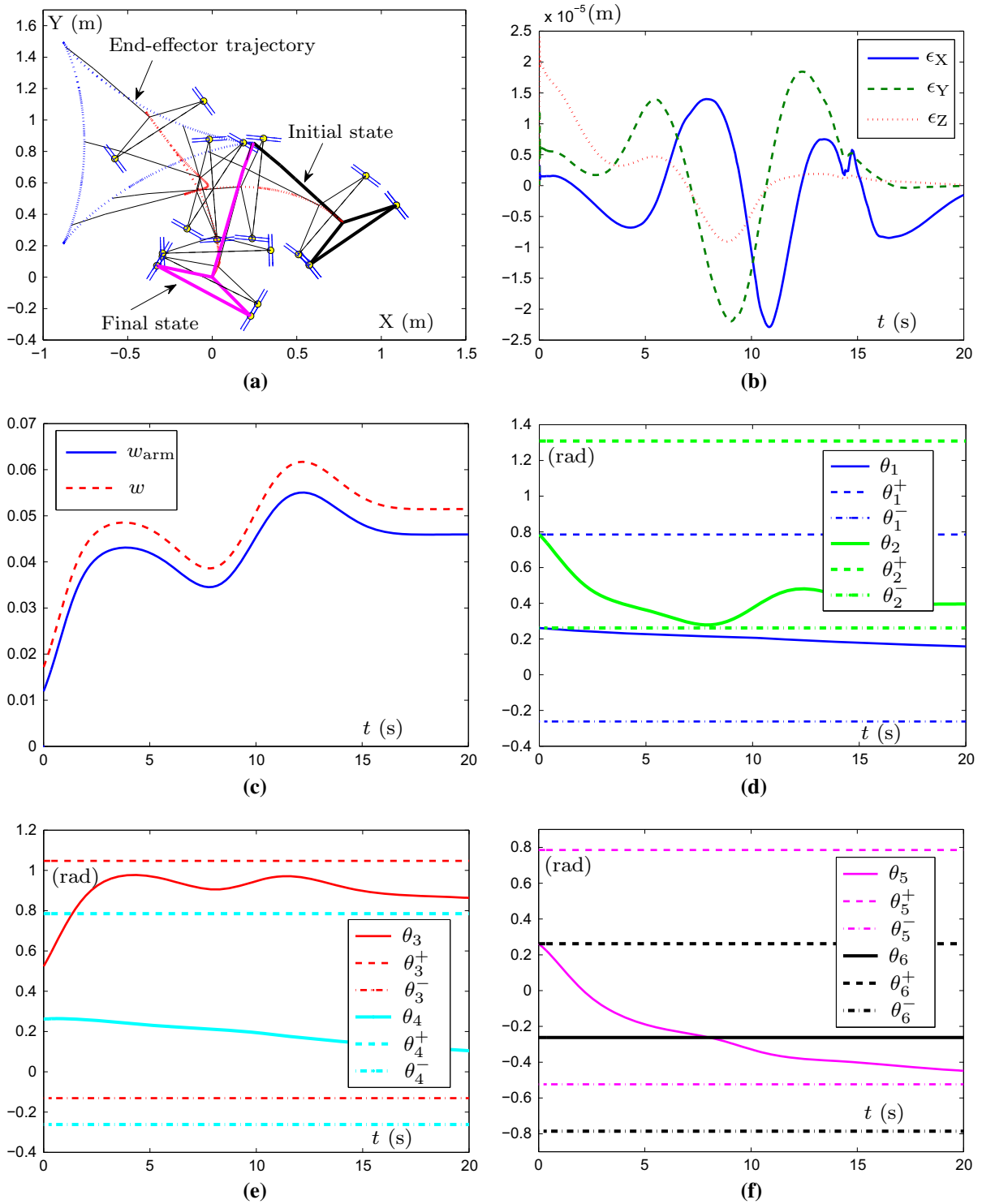


Fig. 5 The WRRM end-effector moves along a tricuspid-curve path, as synthesized by the proposed ReMM scheme (19)–(21) in comparison with Fig. 4. **a** Top view of motion trajectories.

b Position error ϵ profiles. **c** Manipulability measures. **d** Joint angle θ_1 and θ_2 profiles. **e** Joint angle θ_3 and θ_4 profiles. **f** Joint angle θ_5 and θ_6 profiles

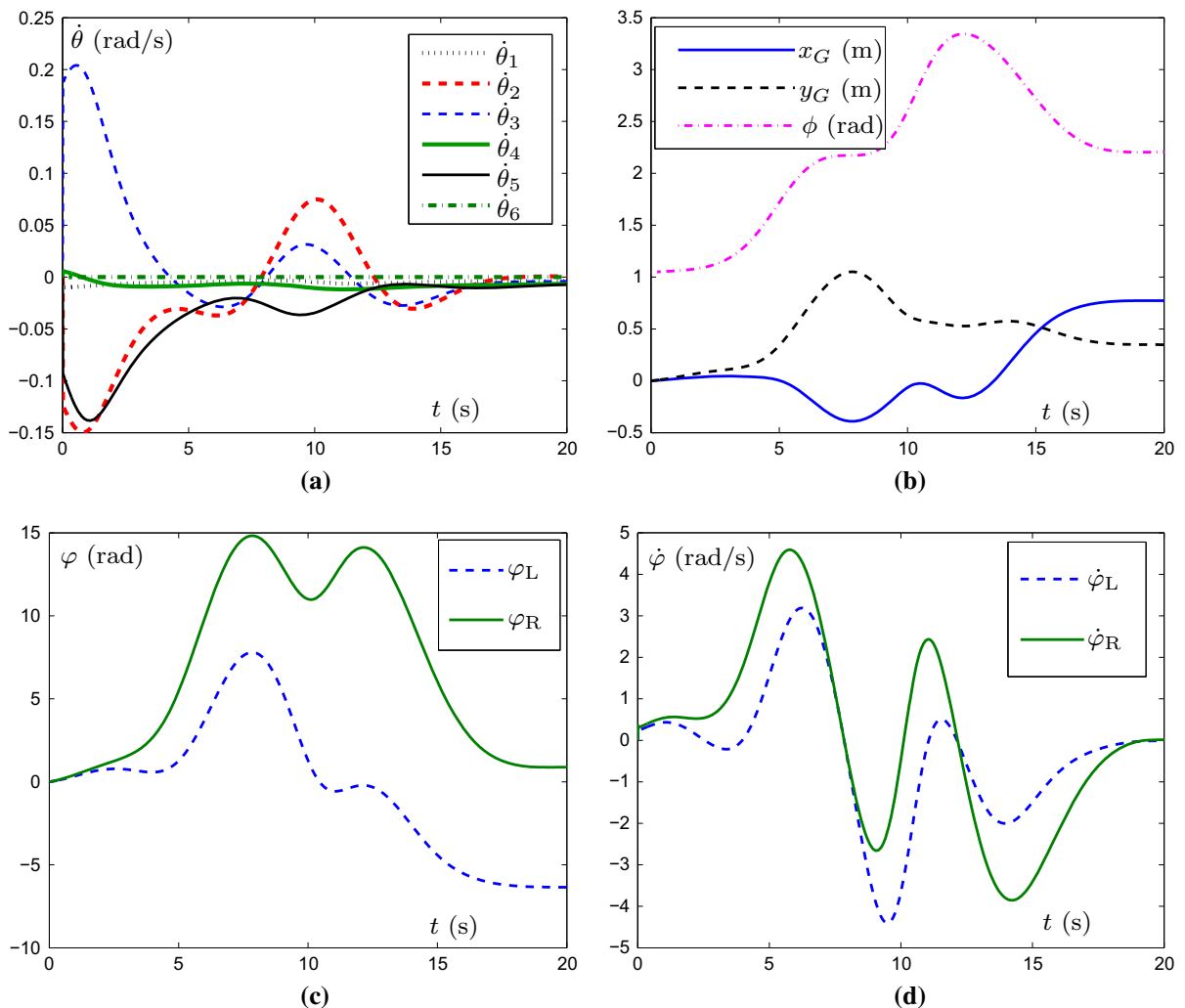


Fig. 6 Supplementary simulation results of the WRM end-effector moves along a tricuspid-curve path, as synthesized by the proposed ReMM scheme (19)–(21) in addition to Fig. 5. **a**

Joint velocity $\dot{\theta}$ profiles. **b** x_G , y_G and ϕ profiles. **c** Rotational angle φ profiles. **d** Rotational velocity $\dot{\varphi}$ profiles

trajectories of the WRM, with the corresponding position error profiles are shown in Fig. 5b. As seen from Fig. 5a, b, the path-tracking task is fulfilled well (with the maximal absolute value of the position error being around 2.5×10^{-5} m) owing to the coordinated motion of the mobile platform and the manipulator. More importantly, as shown in Fig. 5c, the manipulability measures w and w_{arm} are always greater than zero, and, more specifically, greater than their initial values $w(0)$ and $w_{\text{arm}}(0)$, respectively. This implies that the purpose of singularity avoidance is achieved successfully via the proposed ReMM scheme (19)–(21).

Besides, profiles of joint angles are presented in Fig. 5d–f. Evidently, all the synthesized joint angles are kept within their corresponding joint limits and not reach their limits, showing the effectiveness of the bound constraint (21). By comparing Fig. 4 with Fig. 5, the proposed ReMM scheme is superior to the RoMM scheme. For further investigation and illustration, more supplementary simulation results synthesized by the proposed scheme (19)–(21) are shown in Fig. 6. As illustrated in Fig. 6, the profiles of $\dot{\theta}$, x_G , y_G , ϕ , φ and $\dot{\varphi}$ vary with time t continuously and smoothly, which are suitable for practical applications. Moreover, as compared to

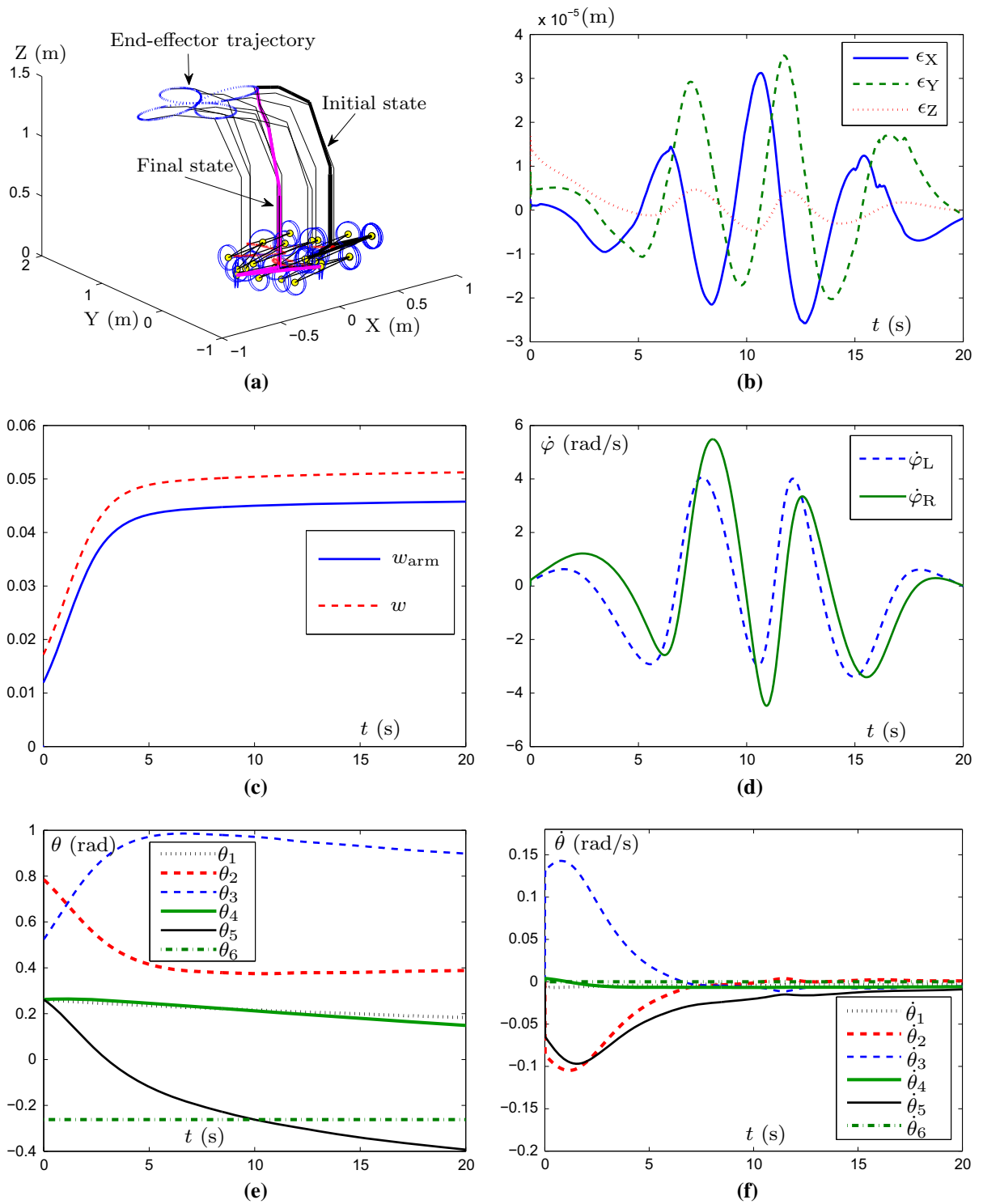


Fig. 7 The WRRM end-effector moves along a Rhodonea-curve path with $\sigma = 2$, as synthesized by the proposed ReMM scheme (19)–(21). **a** Motion trajectories. **b** Position error ϵ profiles. **c**

Manipulability measures. **d** Rotational velocity $\dot{\varphi}$ profiles. **e** Joint angle θ profile. **f** Joint velocity $\dot{\theta}$ profiles

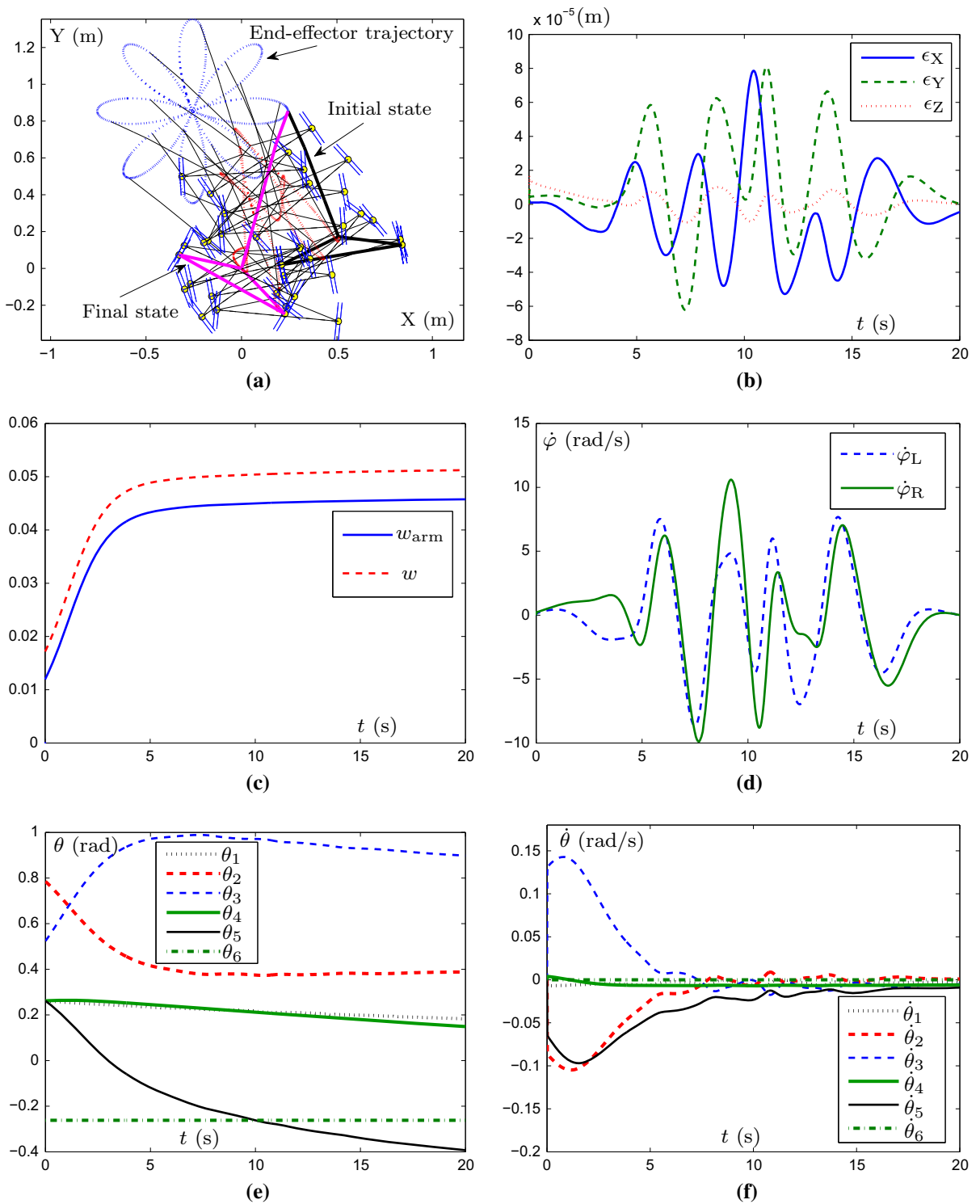


Fig. 8 The WRRM end-effector moves along a Rhodonea-curve path with $\sigma = 4$, as synthesized by the proposed ReMM scheme (19)–(21). **a** Top view of motion trajectories. **b** Position error ϵ

profiles. **c** Rotational velocity $\dot{\varphi}$ profiles. **d** Rotational velocity $\dot{\varphi}$ profiles. **e** Joint angle θ profiles. **f** Joint velocity $\dot{\theta}$ profiles

physical limits listed in Table 2, all the joint velocities and rotational velocities are kept within their physical limits [showing again the effectiveness of the bound constraint (21)]. All these results further demonstrate the efficacy of the proposed ReMM scheme.

In summary, the above simulation results have demonstrated the efficacy, accuracy and superiority of the proposed ReMM scheme (19)–(21) for manipulability maximizing and coordinated motion planning and control of the WMRM, as compared to the RoMM scheme (15)–(18).

5.2 Rhodonea-curve path-tracking tasks

In this subsection, the end-effector is expected to track a Rhodonea-curve path [47], which is synthesized by the proposed ReMM scheme (19)–(21). Similarly, for better understanding, the desired velocities of the manipulator's end-effector for tracking the Rhodonea-curve path are designed as

$$\begin{cases} \dot{r}_{dwX} = -\alpha \frac{\pi^2}{T} \sin\left(\frac{\pi t}{T}\right) (\sigma \sin(\sigma\beta) \cos(\beta) \\ \quad + \cos(\sigma\beta) \sin(\beta)), \\ \dot{r}_{dwY} = -\alpha \frac{\pi^2}{T} \sin\left(\frac{\pi t}{T}\right) (\sigma \sin(\sigma\beta) \sin(\beta) \\ \quad - \cos(\sigma\beta) \cos(\beta)), \\ \dot{r}_{dwZ} = 0, \end{cases}$$

where $\alpha = 0.5$ and $\beta = 2\pi \sin^2(\pi t/(2T))$ are used in this paper. Note that different values of σ would lead to different types of Rhodonea curves [47]. In the simulations, $\sigma = 2$ and $\sigma = 4$ are used for investigation and illustration, and the corresponding simulation results are shown in Figs. 7 and 8.

As seen from Figs. 7a, b, and 8a, b, by using the proposed ReMM scheme (19)–(21), the two desired Rhodonea-curve paths are tracked successfully, with the maximal absolute value of position errors being tiny enough (e.g., less than 8.0×10^{-5} m). In addition, from Figs. 7c and 8c, we can also observe that, when the manipulator's end-effector tracks the Rhodonea curve with $\sigma = 2$ or $\sigma = 4$, the manipulability measures w and w_{arm} are always greater than their initial value $w(0)$ and $w_{arm}(0)$, respectively. More specifically, w and w_{arm} keep increasing during the end-effector task execution, which implies that there does not exist the singularity problem in coordinated motion planning and control of the WMRM. In the two path-tracking tasks, all the joint angles, joint velocities and

rotational velocities illustrated in Figs. 7b–f and 8b–f are kept within their corresponding physical limits shown in Table 2. These results demonstrate well the efficacy of the proposed ReMM scheme (19)–(21) for coordinated motion planning and control of the WMRM.

In summary, all the above simulation results (i.e., Figs. 4, 5, 6, 7 and 8) have demonstrated well that the proposed ReMM scheme (19)–(21) is effective on maximizing the manipulability of the WMRM system and the six-DOF manipulator.

6 Conclusions

By following the pseudoinverse-type formulation (8), this paper has proposed and investigated the novel manipulability-maximizing scheme, i.e., the ReMM scheme (19)–(21), for the coordinated motion planning and control of the WMRM. Then, such a scheme, which treats the mobile platform and the redundant manipulator as a combined system and incorporates position feedback and physical limits, has been reformulated into a unified QP. For testing the proposed ReMM scheme, a wheeled mobile redundant manipulator composed of a two-wheel-drive mobile platform and a six-DOF manipulator has been presented and investigated, together with its kinematics analysis. Comparative simulation results based on the presented mobile manipulator have further substantiated the efficacy and superiority of the proposed ReMM scheme for singularity avoidance, physical limits avoidance, and manipulability maximizing of the whole mobile manipulator and the six-DOF manipulator. Besides, it is worth pointing out that the proposed ReMM scheme can both be suitable for the presented wheeled mobile manipulator and be applied to other types of mobile manipulators, which can be an interesting direction of the future work.

Acknowledgments This work is supported by the National Natural Science Foundation of China (with number 61473323), by the Foundation of Key Laboratory of Autonomous Systems and Networked Control, Ministry of Education, China (with number 2013A07), and also by the Science and Technology Program of Guangzhou, China (with number 2014J4100057). Besides, the authors would like to thank the editor(s) and anonymous reviewer(s) for the time and effort spent in handling the paper, as well as many constructive comments provided for improving the presentation and quality of the paper.

Appendix

In this appendix, the detailed expression of the matrix $J(\vartheta)$ in (6) is presented. First, we denote $J(\vartheta)$ as

$$J(\vartheta) = \begin{bmatrix} j_{11} & j_{12} & j_{13} & j_{14} & j_{15} & j_{16} & j_{17} & j_{18} \\ j_{21} & j_{22} & j_{23} & j_{24} & j_{25} & j_{26} & j_{27} & j_{28} \\ j_{31} & j_{32} & j_{33} & j_{34} & j_{35} & j_{36} & j_{37} & j_{38} \end{bmatrix} \in R^{m \times (2+n)}.$$

Second, let

$$j_{01} = l_{65}(-c_5 s_{32} s_{1\phi} + s_5 c_4 c_{32} s_{1\phi} + s_5 s_4 c_{1\phi}) - l_{43} s_{32} s_{1\phi} - l_2 s_2 s_{1\phi},$$

and

$$j_{02} = l_{65}(c_5 s_{32} c_{1\phi} - s_5 c_4 c_{32} c_{1\phi} + s_5 s_4 s_{1\phi}) + l_{43} s_{32} c_{1\phi} + l_2 s_2 c_{1\phi}.$$

Then, the elements of $J(\vartheta)$ are shown as follows:

$$j_{11} = \frac{\gamma}{2} c_\phi + \frac{\gamma d}{2b} s_\phi - \frac{\gamma}{2b} j_{01},$$

$$j_{12} = \frac{\gamma}{2} c_\phi - \frac{\gamma d}{2b} s_\phi + \frac{\gamma}{2b} j_{01},$$

$$j_{13} = j_{01},$$

$$j_{14} = l_{65}(c_5 c_{32} c_{1\phi} + s_5 c_4 s_{32} c_{1\phi}) + l_{43} c_{32} c_{1\phi} + l_2 c_2 c_{1\phi},$$

$$j_{15} = l_{65}(c_5 c_{32} c_{1\phi} + s_5 c_4 s_{32} c_{1\phi}) + l_{43} c_{32} c_{1\phi},$$

$$j_{16} = l_{65}(s_5 s_4 c_{32} c_{1\phi} + s_5 c_4 s_{1\phi}),$$

$$j_{17} = l_{65}(-s_5 s_{32} c_{1\phi} - c_5 c_4 c_{32} c_{1\phi} + c_5 s_4 s_{1\phi}),$$

$$j_{18} = 0;$$

$$j_{21} = \frac{\gamma}{2} s_\phi - \frac{\gamma d}{2b} c_\phi - \frac{\gamma}{2b} j_{02},$$

$$j_{22} = \frac{\gamma}{2} s_\phi + \frac{\gamma d}{2b} c_\phi + \frac{\gamma}{2b} j_{02},$$

$$j_{23} = j_{02},$$

$$j_{24} = l_{65}(c_5 c_{32} s_{1\phi} + s_5 c_4 s_{32} s_{1\phi}) + l_{43} c_{32} s_{1\phi} + l_2 c_2 s_{1\phi},$$

$$j_{25} = l_{65}(c_5 c_{32} s_{1\phi} + s_5 c_4 s_{32} s_{1\phi}) + l_{43} c_{32} s_{1\phi},$$

$$j_{26} = l_{65}(s_5 s_4 c_{32} s_{1\phi} - s_5 c_4 c_{1\phi}),$$

$$j_{27} = l_{65}(-s_5 s_{32} s_{1\phi} - c_5 c_4 c_{32} s_{1\phi} - c_5 s_4 c_{1\phi}),$$

$$j_{28} = 0;$$

$$j_{31} = j_{32} = j_{33} = 0,$$

$$j_{34} = l_{65}(s_5 c_4 c_{32} - c_5 s_{32}) - l_{43} s_{32} - l_2 s_2,$$

$$j_{35} = l_{65}(s_5 c_4 c_{32} - c_5 s_{32}) - l_{43} s_{32},$$

$$j_{36} = l_{65}(-s_5 s_4 s_{32}),$$

$$j_{37} = l_{65}(c_5 c_4 s_{32} - s_5 c_{32}),$$

$$j_{38} = 0,$$

where $\gamma = 0.1025$ m, $b = 0.32$ m, and $d = 0.1$ m.

References

- Pan, H., Xin, M.: Nonlinear robust and optimal control of robot manipulators. *Nonlinear Dyn.* **76**, 237–254 (2014)
- Guo, D., Zhang, Y.: Simulation and experimental verification of weighted velocity and acceleration minimization for robotic redundancy resolution. *IEEE Trans. Autom. Sci. Eng.* **11**, 1203–1217 (2014)
- Guo, D., Zhang, Y.: Acceleration-level inequality-based man scheme for obstacle avoidance of redundant robot manipulators. *IEEE Trans. Ind. Electron.* **61**, 6903–6914 (2014)
- Werfel, J., Petersen, K., Nagpal, R.: Designing collective behavior in a termite-inspired robot construction team. *Science* **343**, 754–758 (2014)
- Korayem, M.H., Tourajizadeh, H., Zehfroosh, A., Korayem, A.H.: Optimal path planning of a cable-suspended robot with moving boundary using optimal feedback linearization approach. *Nonlinear Dyn.* **78**, 1515–1543 (2014)
- Izadbakhsh, A., Fateh, M.M.: Real-time robust adaptive control of robots subjected to actuator voltage constraint. *Nonlinear Dyn.* **78**, 1999–2014 (2014)
- Saedi, S., Paull, L., Trentini, M., Seto, M., Li, H.: Group mapping: a topological approach to map merging for multiple robots. *IEEE Robot. Autom. Mag.* **21**, 60–72 (2014)
- Korayem, M.H., Nazemzadeh, M., Nohooji, H.R.: Optimal point-to-point motion planning of non-holonomic mobile robots in the presence of multiple obstacles. *J. Braz. Soc. Mech. Sci. Eng.* **36**, 221–232 (2014)
- Siciliano, B., Khatib, O.: *Springer Handbook of Robotics*. Springer, Heidelberg (2008)
- Yuan, J., Chen, H., Sun, F., Huang, Y.: Trajectory planning and tracking control for autonomous bicycle robot. *Nonlinear Dyn.* **78**, 421–431 (2014)
- Urakubo, T.: Feedback stabilization of a nonholonomic system with potential fields: application to a two-wheeled mobile robot among obstacles. *Nonlinear Dyn.* **81**, 1475–1487 (2015)
- Zhang, Z., Zhang, Y.: Repetitive motion planning and control on redundant robot manipulators with push-rod-type joints. *ASME J. Dyn. Syst., Meas. Control* **135**, 024502 (2013)
- Guo, D., Zhang, Y.: Different-level two-norm and infinity-norm minimization to remedy joint-torque instability/divergence for redundant robot manipulators. *Robot. Auton. Syst.* **60**, 874–888 (2012)
- Hsiao, T., Weng, M.C.: Robust joint position feedback control of robot manipulators. *ASME J. Dyn. Syst. Meas. Control* **135**, 031010 (2013)
- Farmanbordar, A., Hoseini, S.M.: Neural network adaptive output feedback control of flexible link manipulators. *ASME J. Dyn. Syst. Meas. Control* **135**, 021009 (2013)

16. Watanabe, T.: Effect of torque-velocity relationship on manipulability for robot manipulators. *ASME J. Mech. Robot.* **3**, 041007 (2011)
17. Tanaka, Y., Nishikawa, K., Yamada, N., Tsuji, T.: Analysis of operational comfort in manual tasks using human force manipulability measure. *IEEE Trans. Haptics* **8**, 8–19 (2015)
18. Cui, M., Huang, R., Liu, H., Liu, X., Sun, D.: Adaptive tracking control of wheeled mobile robots with unknown longitudinal and lateral slipping parameters. *Nonlinear Dyn.* **78**, 1811–1826 (2014)
19. Fateh, M.M., Arab, A.: Robust control of a wheeled mobile robot by voltage control strategy. *Nonlinear Dyn.* **79**, 335–348 (2015)
20. Zhong, G., Kobayashi, Y., Hoshino, Y., Emaru, T.: System modeling and tracking control of mobile manipulator subjected to dynamic interaction and uncertainty. *Nonlinear Dyn.* **73**, 167–182 (2013)
21. Xiao, L., Zhang, Y.: Solving time-varying inverse kinematics problem of wheeled mobile manipulators using Zhang neural network with exponential convergence. *Nonlinear Dyn.* **76**, 1543–1559 (2014)
22. Chen, H., Wang, C., Yang, L., Zhang, D.: Semiglobal stabilization for nonholonomic mobile robots based on dynamic feedback with inputs saturation. *ASME J. Dyn. Syst. Meas. Control* **134**, 041006 (2012)
23. Olsen, S.G., Bone, G.M.: Development of a hybrid dynamic model and experimental identification of robotic bulldozing. *ASME J. Dyn. Syst. Meas. Control* **135**, 021015 (2013)
24. Tchon, K.: Repeatability of inverse kinematics algorithms for mobile manipulators. *IEEE Trans. Autom. Control* **47**, 1376–1380 (2002)
25. Tchon, K., Jakubiak, J.: A repeatable inverse kinematics algorithm with linear invariant subspaces for mobile manipulators. *IEEE Trans. Syst. Man Cybern. B* **35**, 1051–1057 (2005)
26. Tan, J., Xi, N., Wang, Y.: Integrated task planning and control for mobile manipulators. *Int. J. Robot. Res.* **22**, 337–354 (2003)
27. Bayle, B., Fourquet, J.-Y., Renaud, M.: Manipulability of wheeled mobile manipulators: application to motion generation. *Int. J. Robot. Res.* **22**, 565–581 (2003)
28. Korayem, M.H., Rahimi, H.N., Nikoobin, A.: Mathematical modeling and trajectory planning of mobile manipulators with flexible links and joints. *Appl. Math. Modell.* **36**, 3229–3244 (2012)
29. Nagatani, K., Hirayama, T., Gofuku, A., Tanaka, Y.: Motion planning for mobile manipulator with keeping manipulability. In: *Proceedings of the IEEE/RSJ International Conference on Intelligent Robots and Systems*, pp. 1663–1668 (2002)
30. Yamamoto, Y., Yun, X.: Coordinating locomotion and manipulation of a mobile manipulator. *IEEE Trans. Autom. Control* **39**, 1326–1332 (1994)
31. Liu, Y., Yu, Y., Jiang, C.: Survey of robot manipulability. *Mach. Des. Res.* **19**, 34–37 (2003)
32. Yoshikawa, T.: Analysis and control of robot manipulators with redundancy. In: *Proceedings of the 1st International Symposium on Robotics Research*, pp. 735–747 (1984)
33. Donelan, P.S.: *Singularities of Robot Manipulators*. World Scientific, Hackensack (2007)
34. Huang, Q., Tanie, K., Sugano, S.: Coordinated motion planning for a mobile manipulator considering stability and manipulation. *Int. J. Robot. Res.* **19**, 732–742 (2000)
35. Kobayashi, Y., Minami, M., Yanou, A., Maeba T.: Dynamic reconfiguration manipulability analyses of humanoid bipedal walking. In: *IEEE Robotics and Automation Society. Robotics and Automation*, pp. 4779–4784 (2013)
36. Gu, Y., George Lee, C. S., Yao, B.: Feasible center of mass dynamic manipulability of humanoid robots. In: *IEEE Robotics and Automation Society. Robotics and Automation*, pp. 5082–5087 (2015)
37. Guo, W., Wang, J., Chen, W.: A manipulability improving scheme for opening unknown doors with mobile manipulator. In: *IEEE International Conference on Robotics and Biomimetics*, pp. 1362–1367 (2014)
38. Clingerman, C., Lee, D. D.: Estimating manipulability of unknown obstacles for navigation in indoor environments. In: *Proceedings of the IEEE International Conference on Robotics and Automation*, pp. 2771–2778 (2014)
39. Cai, B., Zhang, Y.: Different-level redundancy-resolution and its equivalent relationship analysis for robot manipulators using gradient-descent and Zhang et al.'s neural-dynamic methods. *IEEE Trans. Ind. Electron.* **59**, 3146–3155 (2012)
40. Zhang, Z., Zhang, Y.: Acceleration-level cyclic-motion generation of constrained redundant robots tracking different paths. *IEEE Trans. Syst. Man Cybern. B* **42**, 1257–1269 (2012)
41. Zhang, Y., Guo, D., Li, K., Li, J.: Manipulability-maximizing self-motion planning and control of redundant manipulators with experimental validation. In: *IEEE International Conference on Mechatronics and Automation*, pp. 1829–1834 (2012)
42. He, B.: Solving a class of linear projection equation. *Numer. Math.* **68**, 71–80 (1994)
43. Zhang, Y.: On the LVI-based primal-dual neural network for solving online linear and quadratic programming problems. In: *Proceedings of the American Control Conference*, pp. 1351–1356 (2005)
44. Xiao, L., Zhang, Y.: Acceleration-level repetitive motion planning and its experimental verification on a six-link planar robot manipulator. *IEEE Trans. Control Syst. Technol.* **21**, 906–914 (2013)
45. Xiao, L., Lu, R.: Finite-time solution to nonlinear equation using recurrent neural dynamics with a specially-constructed activation function. *Neurocomputing* **151**, 246–251 (2015)
46. Bian, W., Chen, X.: Smoothing neural network for constrained non-Lipschitz optimization with applications. *IEEE Trans. Neural Netw. Learn. Syst.* **23**, 399–411 (2012)
47. Gorjanc, S.: Rose surfaces and their visualizations. *J. Geom. Graphics* **30**, 1–9 (2010)